

VID-LLM: A COMPACT VIDEO-BASED 3D MULTIMODAL LLM WITH RECONSTRUCTION-REASONING SYNERGY

Haijier Chen^{1*}, Bo Xu^{1*}, Shoujian Zhang^{1 †}, Haoze Liu¹, Jiaxuan Lin¹, Jingrong Wang²

¹ School of Geodesy and Geomatics, Wuhan University

² School of Architecture and Urban Planning, Shenzhen University

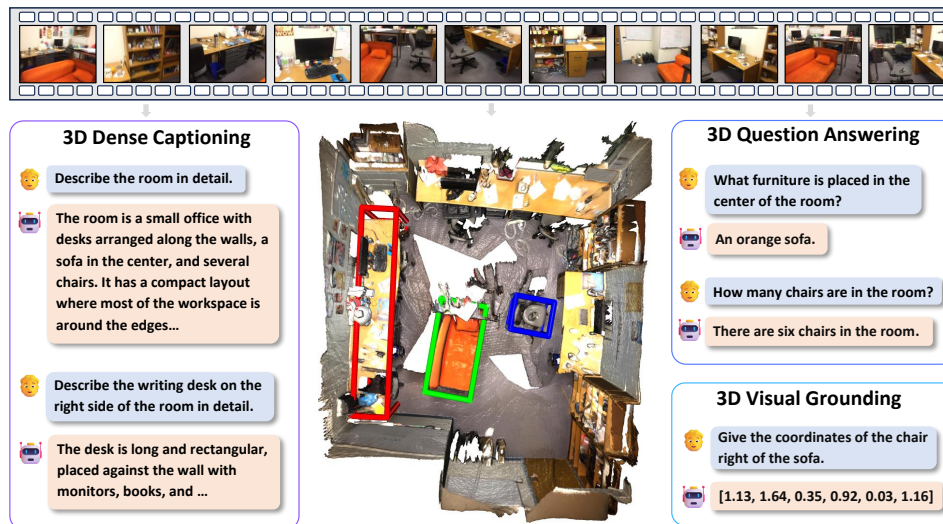


Figure 1: We propose **Vid-LLM** to achieve diverse 3D vision-language reasoning tasks using only video inputs.

ABSTRACT

Recent developments in Multimodal Large Language Models (MLLMs) have significantly improved Vision-Language (VL) reasoning in 2D domains. However, extending these capabilities to 3D scene understanding remains a major challenge. Existing 3D Multimodal Large Language Models (3D-MLLMs) often depend on 3D data inputs, which limits scalability and generalization. To address this limitation, we propose Vid-LLM, a video-based 3D-MLLM that directly processes video inputs without requiring external 3D data, making it practical for real-world deployment. In our method, the geometric prior are directly used to improve the performance of the scene perception. To integrate the geometric cues into the MLLM compactly, we design a Cross-Task Adapter (CTA) module to align the 3D geometric priors with the vision-language representations. To ensure geometric consistency and integrity, we introduce a Metric Depth Model that recovers real-scale geometry from the reconstruction outputs. Finally, the model is fine-tuned with a two-stage distillation optimization strategy, realizing fast convergence and stabilizes training. Extensive experiments across diverse benchmarks verified the effectiveness of our method on 3D Question Answering, 3D Dense Captioning and 3D Visual Grounding tasks, demonstrating the superior multi-task capabilities. Code and data are available on <https://chenhaijier.github.io/Vid-LLM/>.

* Equal contribution.

† Corresponding authors.

1 INTRODUCTION

Recent advances in Large Language Models (LLMs) (Vaswani et al., 2017; Radford et al., 2019; Naveed et al., 2025) and Multimodal Large Language Models (MLLMs) (Zhang et al., 2024a; Yin et al., 2024; Wu et al., 2023) have reinforced the paradigm of language as a universal interface, substantially improving cross-modal perception and reasoning. Extending this progress to 3D, recent research has focused on 3D-aware Multimodal Large Language Models (3D-MLLMs) (Ren et al., 2025), which unify 3D scene understanding and vision–language reasoning under a linguistic interface. This line of work underscores the importance of grounding language in persistent 3D spatial representations (Cheng et al., 2024a; Roh et al., 2022), offering a unified pathway toward systematic scene-level reasoning.

Recent studies have made substantial progress in 3D vision–language (3D VL) reasoning (Chen et al., 2024c; Huang et al., 2023b), yet most approaches rely on complex 3D inputs, incurring high costs in data collection, preprocessing, and computation. Some models rely on point clouds or re-constructed scenes augmented with rendered views or semantic–geometric features (Hong et al., 2023a; Fu et al., 2024), while others adopt simpler inputs but still depend on explicit 3D scene representations such as reconstructed objects aligned with semantic representations (Chu et al., 2024; Huang et al., 2023a; 2024). Despite their effectiveness, these pipelines depend on depth, poses, or external modules, leading to substantial data and engineering overhead as well as high memory and latency costs. This rigid input requirements and system complexity fundamentally limit the scalability and transferability of current 3D-MLLMs.

To overcome these limitations, a more general solution is to enable the model to directly reconstruct scene geometry from video (Leroy et al., 2024; Wang et al., 2024), thereby eliminating the reliance on external depth, pose, or registration modules. More importantly, reconstruction and reasoning are intrinsically interdependent: geometric structures underpin semantic understanding, while semantic reasoning, in turn, provides contextual priors that guide and refine geometric modeling (Cheng et al., 2024a; Ha & Song, 2022).

In this work, we introduce Vid-LLM, a compact model that jointly performs reconstruction and 3D vision–language reasoning from monocular video inputs, as illustrated in Fig. 1. The core component of Vid-LLM is a Cross-Task Adapter (CTA) that tightly couples reconstruction with reasoning, enabling intrinsic geometry–semantics interaction with mutual reinforcement and constraint. CTA disentangles geometry-aware and language-aware features; the geometric stream is then processed by a Global-Frame Attention backbone and specialized heads to estimate camera poses and relative depth, followed by a Metric Depth Model for real-scale calibration. The recovered 3D information is then fused with semantic features to construct 3D patches, which are fed into the LLM for spatial reasoning. Finally, a two-stage training strategy ensures convergence and improves overall performance. Extensive experiments across diverse 3D vision–language benchmarks demonstrate the performance of Vid-LLM and confirm its effectiveness as a practical and scalable framework for video-based 3D multimodal reasoning.

Our main contributions are summarized as follows:

- We propose Vid-LLM for versatile 3D scene understanding. The framework does not rely on dense 3D inputs or prior poses, making it practical for real-world deployment.
- We design a Cross-Task Adapter to align the 3D geometry priors with VL representations, boosting the integration of 3D visual geometry priors into MLLM. A two-stage training strategy is further adopted to improve the stability and performance.
- Extensive experimental evaluations are conducted on real datasets to evaluate the performance of our method. The experimental results demonstrate that our method achieves superior performance in terms of question answering, dense captioning and visual grounding. We will publish our code to facilitate communication.

2 RELATED WORK

3D-MLLMs have achieved significant advances in 3D scene understanding, yet their reliance on explicit 3D data still limits scalability and applicability. Meanwhile, progress in 3D reconstruction

shows that geometry can be directly reconstructed from videos. Integrating such geometric priors into 3D-MLLMs represents a promising approach to enhance semantic grounding. We therefore review related work in three directions: (i) 3D-MLLMs, (ii) 3D reconstruction, and (iii) geometry priors in vision-language models.

3D-aware Multimodal Large Language Models (3D-MLLMs). 3D-MLLMs aim to unify 3D scene understanding and vision–language reasoning within a unified linguistic interface, representing an important extension of multimodal large language models (MLLMs). Existing approaches predominantly rely on explicit geometric inputs: some leverage point clouds or reconstructed scenes, often augmented with rendered views, region-level alignments, or condensed 3D feature grids to support large-scale embodied training (Hong et al., 2023a; Chen et al., 2024b;c; Fu et al., 2024; Huang et al., 2023b); others map 3D features to the language space and model spatial relations to enable interactive dialogue (Huang et al., 2023a; 2024; Zheng et al., 2025b; Huang et al., 2025). Despite their progress, these methods invariably depend on complex inputs such as point clouds, reconstructed scenes, multi-view renderings, or object-level annotations, which impose substantial burdens on data acquisition, preprocessing, and computation, thereby limiting scalability and transferability. In addition, the recent approach VGLLM (Zheng et al., 2025a) explores a video-based 3D-MLLM setting by adopting the geometry encoder of VGGT (Wang et al., 2025a) to extract 3D geometry features from video.

3D Reconstruction. 3D reconstruction has evolved from multi-view geometry pipelines to neural implicit representations and, more recently, feed-forward transformer-based architectures. Classical methods yield accurate geometry but require dense views and heavy preprocessing (Schonberger & Frahm, 2016; Furukawa et al., 2015). Neural radiance fields and point-based extensions improve fidelity and efficiency but focus mainly on appearance modeling while lacking semantic reasoning (Mildenhall et al., 2021; Barron et al., 2022; Kerbl et al., 2023). Recent feed-forward approaches enable direct prediction of depth, pose, and point clouds from video inputs (Wang et al., 2024; Leroy et al., 2024; Wang et al., 2025a). Nevertheless, 3D reconstruction is still only weakly integrated into vision–language research, and its role in supporting semantic reasoning remains underexplored.

Geometry Priors in Vision-Language Models. Incorporating geometry priors has become a key approach for Vision-Language Models (VLMs) to enhance spatial understanding. Along a spectrum of reliance on explicit 3D inputs, existing methods can be organized into three categories: first, explicit input injection, which introduces depth, point clouds, or scene graphs as additional modalities to provide metric properties (Cai et al., 2025; Cheng et al., 2024b; Guo et al., 2023); second, internalization at the data and training level, which leverages spatially annotated corpora or geometric distillation to embed geometry implicitly into the alignment space, enabling spatial reasoning without explicit 3D inputs at inference (Chen et al., 2024a; Peng et al., 2023); and third, modular or prompt-based integration, which augments VLMs with lightweight modules or outputs from 3D foundation models, typically without large-scale retraining (Ma et al., 2024; Kerr et al., 2023). In contrast, our approach generates geometry through a video-driven reconstruction branch and achieves alignment with the semantic branch, enabling a structured and reusable integration of geometry priors within a video-based setting.

3 METHOD

We present Vid-LLM, a video-based 3D multimodal large language model (3D-MLLM). The main components are presented in the following sections: the Cross-Task Adapter is described in Section 3.1, the reconstruction and reasoning branches are detailed in Sections 3.2 and 3.3, and the training strategy is outlined in Section 3.4. The overall architecture is shown in Fig. 2.

3.1 CROSS-TASK ADAPTER

In Vid-LLM, we employ DINOv2 as the shared visual encoder to extract base tokens $T_{base} \in \mathbb{R}^{N \times C}$ from the input image sequence, where N denotes the number of tokens and C is the embedding dimension. To enhance feature effectiveness, we introduce a Cross-Task Adapter (CTA) that aligns 3D geometry priors with vision–language (VL) representations, facilitating the integration of geometric cues into multimodal reasoning.

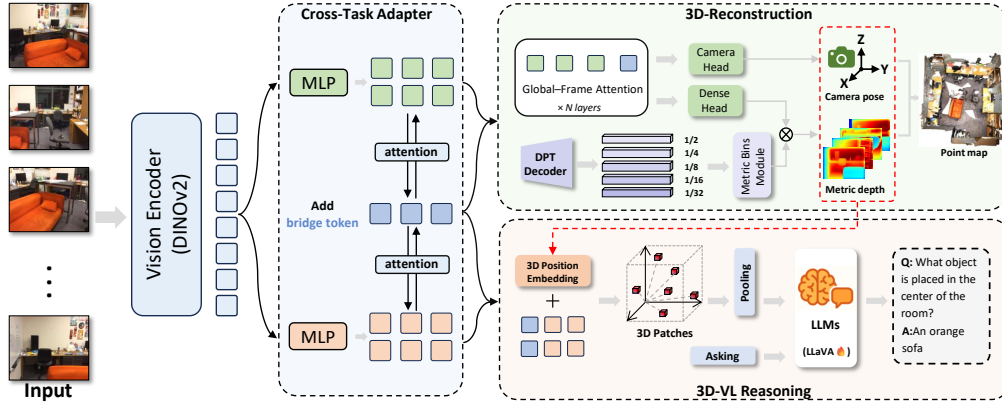


Figure 2: **Architecture of Vid-LLM.** From video, a shared DINOv2 encoder produces tokens that are bidirectionally fused by Cross-Task Adapter with learnable Bridge Tokens, yielding geometric and semantic streams. The reconstruction branch predicts camera poses, depth and recovers real-scale via a Metric-Bins module, while the 3D-VL branch lifts features into 3D tokens for LLM reasoning.

To adapt the shared visual representations for different branches, we employ two lightweight MLP projection heads, $\phi_{geom}(\cdot)$ and $\phi_{lang}(\cdot)$, which map the shared vision tokens to geometry-specific and semantic feature spaces, respectively:

$$T_{geom} = \phi_{geom}(T_{base}), \quad T_{lang} = \phi_{lang}(T_{base}) \quad (1)$$

To effectively align 3D geometry priors with vision–language representations thus enhance the integration of spatial cues into multimodal reasoning, we introduce learnable Bridge Tokens, denoted as $T_{bridge} \in \mathbb{R}^{K \times C}$. Acting as shared memory units, the bridge tokens attend to geometric and semantic features separately, and the updated representation is formulated as:

$$T'_{bridge} = \text{Attn}(T_{bridge}, T_{geom}^{fused}, T_{geom}^{fused}) + \text{Attn}(T_{bridge}, T_{lang}^{fused}, T_{lang}^{fused}) \quad (2)$$

where $\text{Attn}(\cdot)$ denotes a standard multi-head attention operation. This operation enables bridge tokens to dynamically capture complementary information from both tasks and update their representations during training. The joint propagation of geometric and semantic signals strengthens the alignment of 3D geometry priors with vision–language features, leading to more robust cross-modal representations.

Finally, the updated bridge tokens T'_{bridge} are integrated into the feature streams, yielding enhanced task-specific representations T'_{geom} and T'_{lang} . These enriched features capture complementary geometric and semantic cues and are subsequently passed to the reconstruction and reasoning branches. In essence, the Cross-Task Adapter establishes intrinsic geometry–semantics interaction at the feature level, allowing the two streams to reinforce and guide each other for more robust representations.

3.2 3D RECONSTRUCTION MODEL

In the reconstruction branch of Vid-LLM, we build on recent transformer-based architectures for end-to-end 3D reconstruction (Wang et al., 2025a) to recover scene geometry from video inputs. To additionally recover real-scale information, we design a Metric Depth Model that provides robust global scale cues, enabling reconstructions with both fine structural details and metric consistency.

Geometry Encoding and Prediction Heads. Based on the cross-task enhanced geometric features T'_{geom} , together with camera tokens T^{cam} and register tokens T^{reg} , the Global-Frame Attention backbone produces an integrated geometric representation, which is then fed into two prediction heads: a camera head estimating intrinsic-extrinsic parameters and a DPT head that predicts the relative depth map $\hat{D}_{rel} \in \mathbb{R}^{H \times W}$, where H and W denote the image height and width, respectively.

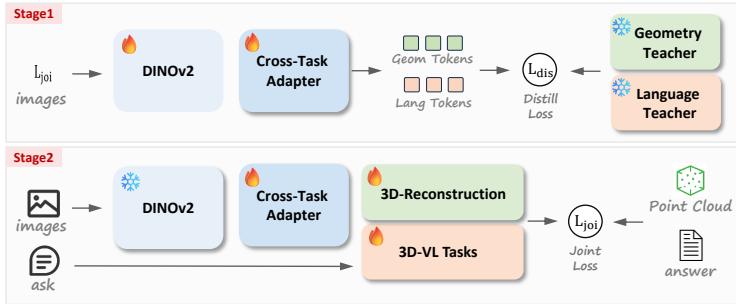


Figure 3: **Overview of the two-stage training strategy.** Stage-1 employs dual-teacher distillation to align geometry and semantics, and Stage-2 jointly optimizes reconstruction and 3D vision–language tasks.

Metric Depth Model. To recover real-scale geometry, we equip the DINOv2 features with a DPT-style decoder that produces multi-scale depth representations. Each pixel’s depth is modeled using a bin-based formulation, where the probability $p_i(k)$ over the k -th bin and its refined center $c_i(k)$ jointly determine the prediction as $\hat{d}(i) = \sum_{k=1}^N p_i(k) c_i(k)$. We use an ordinal-aware normalization to capture relative depth ordering. To further stabilize scale, the bin centers $c_i(k)$ are adaptively refined as $c_i(k) = c_k + \Delta c_i(k)$, where $\Delta c_i(k) = r_k(F_i)$ is predicted from the decoder features F_i . The resulting metric depth map $\hat{D}_{\text{metric}} = \{\hat{d}(i)\}_{i=1}^{H \times W}$ provides global scale cues that are aligned with relative predictions for real-scale reconstruction.

Real-Scale Alignment. We estimate a scaling factor between the relative depth \hat{D}_{rel} predicted by the DPT head and the metric depth \hat{D}_{metric} predicted by the Metric Depth Model via weighted least squares. For each scene, 16 images are randomly sampled to compute per-image scaling factors, and their median is taken as the final scene-level factor. This factor is then applied to convert both the relative depth and the predicted camera pose into real-world units. Rather than directly using metric depth as the final output, we adopt this alignment strategy since the DPT head provides more accurate texture details compared with the Metric Depth Model, which could also be observed from experimental results.

3.3 3D VISION–LANGUAGE MODEL

In the reasoning branch of Vid-LLM, cross-task-enhanced semantic features T'_{lang} are combined with reconstructed geometry to generate dense 3D patch representations, which are then fed into the LLM for 3D question answering, grounding, and captioning tasks.

3D Patch Construction. Each 2D feature $T'_{\text{lang}}(i, j)$ is back-projected into 3D using the estimated depth \hat{D} , camera pose (\hat{R}, \hat{t}) and intrinsics K produced by the 3D Reconstruction Model, yielding its camera-frame coordinates $P_v(i, j)$ as:

$$P_v(i, j) = \hat{R}^{-1} K^{-1} [i, j, 1]^T \hat{D}(i, j) - \hat{R}^{-1} \hat{t} \quad (3)$$

These coordinates are encoded by an MLP into positional embeddings $P'_v(i, j)$ that match the dimensionality of the semantic features. Therefore, the final 3D patch tokens are then obtained by fusing geometry and semantic features:

$$T_{3D}(i, j) = T'_{\text{lang}}(i, j) + P'_v(i, j) \quad (4)$$

This operation feeds spatial information into the semantic tokens, further enhancing the spatial awareness in the LLM.

3.4 TRAINING STRATEGY

We adopt a two-stage training strategy to utilize the shared encoder for both geometry and semantics. Stage 1 performs dual-teacher distillation, transferring geometric priors from a reconstruction model and semantic knowledge from a multimodal LLM, enabling the encoder to learn both capabilities in a balanced way. Stage 2 jointly optimizes all downstream modules with 3D vision–language

objectives, while incorporating auxiliary reconstruction losses to provide the model with sufficient reconstruction capability and ensure real-scale consistency. The overall pipeline is illustrated in Fig. 3.

Stage-1 Dual-Teacher Distillation. In stage 1, we adopt a dual-teacher distillation strategy to jointly train the DINO encoder and the Cross-Task Adapter, enabling the modules to quickly learn both geometric and semantic representations. The pretrained DINO encoder and CLIP encoder serve as the geometry and semantic teachers in the distillation strategy, which are initialized from VGGT (Wang et al., 2025a) and LLaVA-3D (Zhu et al., 2025), respectively. The distillation loss is defined as:

$$L_{distill} = L_{geo}^{feat} + L_{lang}^{feat} + \lambda L_{sc} \quad (5)$$

where L_{geo}^{feat} , L_{lang}^{feat} and L_{sc} are the geometry loss, semantic loss and structural consistency loss, respectively. λ is a balancing hyperparameter. For geometry learning, an L2 loss is applied to patch-level features, following DINO’s patch regression strategy. For semantic learning, a cosine similarity loss is applied to pooled features to align with CLIP’s global semantic embedding space. The specific forms are defined as follows:

$$L_{geo}^{feat} = \frac{1}{N} \sum_{i=1}^N \|\text{Norm}(T'_{geom,i}) - \text{Norm}(T_{tea,i}^{geo})\|_2^2, \quad L_{lang}^{feat} = 1 - \cos(\text{Pool}(T'_{lang}), \text{Pool}(T_{tea}^{lang})) \quad (6)$$

where $\text{Norm}(\cdot)$ denotes L2 normalization, and $\text{Pool}(\cdot)$ indicates mean pooling. T'_{geom} and T'_{lang} are the task-specific geometric and semantic features extracted by the Cross-Task Adapter, and serve as the student representations in the distillation strategy. T_{tea}^{geom} and T_{tea}^{lang} are features from the DINO and CLIP encoders and serve as teacher representations. N represents the number of tokens in T'_{geom} . Before computing L_{geo}^{feat} and L_{lang}^{feat} , we apply lightweight linear projection layers to align the features to the same embedding dimension. To maintain structural consistency, we also introduce the structural consistency loss L_{sc} , which is defined as:

$$L_{sc} = \frac{1}{M^2} \|S_{stu} - S_{tea}\|_F^2, \quad \text{where } S_{stu} = Z_{stu} Z_{stu}^\top, S_{tea} = Z_{tea} Z_{tea}^\top \quad (7)$$

$Z_{stu} = [\text{Norm}(T'_{geom}); \text{Norm}(T'_{lang})] \in \mathbb{R}^{M \times C}$ is obtained by concatenating the geometry and semantic tokens from the student representation. $Z_{tea} = [\text{Norm}(T_{tea}^{geo}); \text{Norm}(T_{tea}^{lang})]$ is defined in the same way as Z_{stu} , but using the teacher representation. $\|\cdot\|_F$ is the Frobenius norm, M is the total number of tokens, and C is the embedding dimension of each token.

Stage-2 Joint Optimization. In Stage 2, we further fine-tune all the modules to optimize overall performance. The joint loss is defined as:

$$L_{joint} = L_{recon-task} + L_{VL-task} + L_{MD} \quad (8)$$

where $L_{recon-task}$ is the multi-task loss for 3D reconstruction, consisting of the camera loss, depth loss, and point map loss following Wang et al. (2025a). $L_{VL-task}$ supervises 3D vision-language reasoning, including cross-entropy loss for instruction-following tasks, along with bounding box regression and matching losses for grounding (Zhu et al. (2025)). L_{MD} represents the metric depth loss, combining a global scale penalty and a robust local refinement term, and is defined as:

$$L_{MD} = b^2 + \frac{1}{K} \sum_{i=1}^K \frac{(e_i - b)^2}{1 + \alpha |e_i - b|}, \quad (9)$$

The log-depth error is defined as $e_i = \log(d_i^{pred} + \varepsilon) - \log(d_i^{gt} + \varepsilon)$, where ε is a small constant for numerical stability. $b = \frac{1}{K} \sum_{i=1}^K e_i$ is the mean error across all K valid pixels in the image. The parameter $\alpha > 0$ controls the robustness by down-weighting large residuals.

During joint training, $L_{recon-task}$ and L_{MD} optimize the 3D reconstruction model, $L_{VL-task}$ optimize the 3D vision-language model, while the shared CTA is jointly optimized by $L_{recon-task}$ and $L_{VL-task}$. It is worth noticing that the loss constructed in the 3D-VL reasoning branch is not used to optimize the 3D reconstruction model, which can be seen in Fig. 2. This one-way gradient flow ensures that the CTA acts as a stable bridge for geometry-semantics interaction, enabling effective feature exchange.

Table 1: **Evaluation of 3D Question Answering on ScanQA and SQA3D.** Methods marked with * are 3D MLLM evaluated in video mode. † indicates the model consumes VGGT-generated 3D geometry. "C" stands for "CIDEr", "B-4" for "BLEU-4", "M" for "METEOR", "R" for "ROUGE", and "EM@1" for top-1 exact match.

Method	ScanQA				SQA3D	
	C†	B-4†	M†	R†	EM@1†	EM@1†
<i>3D-based models</i>						
Scan2Cap	–	–	–	–	–	41.0
ScanQA	64.9	10.1	13.1	33.3	21.1	47.2
3D-VisTA	69.6	10.4	13.9	35.7	22.4	48.5
3D-LLM	69.4	12.0	14.5	35.7	20.5	–
LL3DA	76.8	13.5	15.9	37.3	–	–
Grounded3D-LLM	75.9	13.2	–	–	–	–
Chat-3D v2	77.1	7.3	16.1	40.1	21.1	–
Scene-LLM	80.0	12.0	16.6	40.0	27.2	54.2
ChatScene	87.7	14.3	18.0	41.6	21.6	54.6
LEO	101.4	13.2	20.0	49.2	24.5	50.0
Video-3D LLM	102.6	16.2	19.8	49.0	30.1	58.6
LLaVA-3D	103.1	16.4	20.8	49.6	30.6	60.1
3DRS	104.8	17.2	20.5	49.8	30.3	60.6
<i>Video-based models</i>						
VILA-40B	48.2	9.9	11.4	27.3	17.2	37.2
IXC-2.5-7B	53.9	8.7	13.2	31.5	19.4	41.5
LLaVA-OV-7B	78.2	13.3	17.2	40.5	22.9	47.6
LLaVA-Video-7B	88.7	–	–	–	–	48.5
Uni3DR ^{2*}	70.3	12.2	14.9	36.3	17.3	–
ChatScene*	85.6	–	–	–	–	52.9
3DRS†	94.7	12.3	15.9	45.1	23.9	54.5
Vid-LLM (Ours)	101.9	15.8	18.3	49.5	27.6	57.3

Table 2: **Evaluation of 3D Dense Captioning on Scan2Cap.** The n-gram metrics for Scan2Cap are governed by IoU@0.5.

Method	Scan2Cap			
	C@0.5†	B-4@0.5†	M@0.5†	R@0.5†
<i>3D-based models</i>				
Scan2Cap	39.1	23.3	22.0	44.8
Grounded3D-LLM	70.2	35.0	–	–
LEO	68.4	36.9	27.7	57.8
ChatScene	77.1	36.3	28.0	58.1
Video-3D LLM	83.8	42.4	28.9	62.3
LLaVA-3D	84.1	42.6	29.0	63.4
3DRS	86.1	41.6	28.9	62.3
<i>Video-based models</i>				
3DRS†	76.4	39.6	27.3	57.1
VGLLM	78.6	40.9	28.6	62.4
Vid-LLM (Ours)	81.5	40.9	28.7	61.8

Table 3: **Evaluation of 3D Visual Grounding on ScanRefer and Multi3DRefer.**

Method	ScanRefer		Multi3DRefer	
	Acc@0.25†	Acc@0.5†	Acc@0.25†	Acc@0.5†
<i>3D-based models</i>				
ScanRefer	37.3	24.3	–	–
Chat-3D v2	35.9	30.4	–	–
Grounded3D-LLM	48.6	44.0	44.7	40.8
LLaVA-3D	50.1	42.7	49.8	43.6
ChatScene	55.5	50.2	57.1	52.4
Video-3D LLM	58.1	51.7	58.0	52.7
3DRS	62.9	56.1	60.4	54.9
<i>Video-based models</i>				
VGLLM	53.5	47.5	–	–
3DRS†	55.2	51.1	52.8	48.3
Vid-LLM (Ours)	63.2	56.4	61.6	56.1

4 EXPERIMENTS

This section provides a comprehensive evaluation of Vid-LLM. In Section 4.1, we introduce the experimental setup, covering the training details of Vid-LLM and the evaluation settings used in our experiments. In Section 4.2, we evaluate the model on 3D vision–language reasoning tasks against state-of-the-art methods. In Section 4.3, we compare Vid-LLM with representative joint reconstruction–reasoning models to examine how different design choices affect performance when jointly executing reconstruction and 3D VL reasoning. In Section 4.4, we conduct ablation studies to analyze the contributions of core modules.

4.1 EXPERIMENTAL SETUP

Training Details. We adopt DINOv2-L as the visual backbone, consisting of 24 Transformer layers with a hidden dimension of 1024. The projection MLPs use two fully connected layers with an expansion factor of 4 and GELU activation. For data processing, we uniformly sample 32 frames per scene, resize the shorter side to 518, crop the resolution so that both height and width are multiples of 14. Optimization is performed using AdamW with $\beta_1 = 0.9$, $\beta_2 = 0.999$, and weight decay of 0.05, with gradient clipping at 1.0.

Evaluation Details. We follow the standard evaluation protocols and metrics defined for each dataset. For tables that summarize performance across multiple datasets (e.g., Tables 5 and 6), the reported numbers are computed as the mean of the metrics for each benchmark. For the Scan2Cap dataset, we follow prior work (Zhu et al., 2025; Zheng et al., 2025a): instance proposals are generated using Mask3D (Schult et al., 2022), and 3D coordinate tokens are constructed from the predicted instance centers to enable instance-aware caption generation. For the ScanRefer dataset, Mask3D (Schult et al., 2022) serves as the 3D segmentor to remain consistent with supervised baselines (Huang et al., 2024; Chen et al., 2024c; Huang et al., 2023a). For the Nr3D and Sr3D datasets, the provided segmentation annotations are adopted to align with previous methods (Chen et al., 2022; Huang et al., 2023a). For reconstruction evaluation on ScanNet, the metrics are computed in metric scale. All models are trained with the same data and settings for a fair comparison.

4.2 3D VISION–LANGUAGE REASONING

Overview. To comprehensively assess the performance of Vid-LLM on 3D vision–language reasoning tasks, we conduct experiments using widely adopted datasets covering three task categories: 3D Question Answering on ScanQA (Azuma et al., 2022) and SQA3D (Ma et al., 2022), 3D Dense Captioning on Scan2Cap (Chen et al., 2021), and 3D Visual Grounding on ScanRefer (Chen et al., 2020), Multi3DRefer (Zhang et al., 2023), and Nr3D/Sr3D (Achlioptas et al., 2020b).

Baseline. We compare Vid-LLM with a broad set of 3D-based and video-based vision–language reasoning models. 3D-based methods rely on explicit 3D scene inputs such as point clouds or reconstructed geometry, whereas video-based methods operate solely on video. The 3D-based baselines include ScanQA (Azuma et al., 2022), Scan2Cap (Chen et al., 2021), 3D-VisTA (Zhu et al., 2023), 3D-LLM (Hong et al., 2023b), LL3DA (Chen et al., 2024b), Grounded3D-LLM (Chen et al., 2024c), Chat-3D v2 (Huang et al., 2023a), LEO (Huang et al., 2023b), Scene-LLM (Fu et al., 2024), ChatScene (Huang et al., 2024), LLaVA-3D (Zhu et al., 2025), Video-3D LLM (Zheng et al., 2025b), and 3DRS (Huang et al., 2025). The video-based baselines include VILA-40B (Lin et al., 2024), IXC (Zhang et al., 2024b), LLaVA-OV (Li et al., 2024), LLaVA-Video (LLaVA Team, 2024), Uni3DR2 (Chu et al., 2024), and VG-LLM (Zheng et al., 2025a). To further assess the grounding capability of Vid-LLM, we additionally compare against task-specific 3D visual grounding models, including ScanRefer (Chen et al., 2020), 3D-VisTA (Zhu et al., 2023), ReferIt3D (Achlioptas et al., 2020a), 3DVG-Trans (Zhao et al., 2021), MVT (Huang et al., 2022), ViL3DRel (Chen et al., 2022), and SceneVerse (Jia et al., 2024). To allow comparison under the same video input setting with the most competitive 3D-based baseline in our evaluation, we additionally include 3DRS[†], a variant of 3DRS that takes VGGT-generated 3D geometry as input. These comparisons collectively provide a comprehensive evaluation of Vid-LLM across 3D vision–language reasoning tasks.

Result & Analysis. Vid-LLM consistently shows robust performance across all 3D vision–language reasoning benchmarks. As shown in Tab. 1, Vid-LLM achieves the best results among video-based models on both ScanQA and SQA3D, outperforming the second-best baseline (3DRS[†]) by an average margin of 11%. Tab. 2 further shows that Vid-LLM attains the highest performance among video-based methods on Scan2Cap; notably, its M@0.5 score (28.7) is close to that of the best-performing 3D-based model (29.0), despite not using depth or point clouds. These results collectively indicate that the integration of geometric cues into semantic reasoning can significantly improve perception performance. Tab. 3 and Tab. 4 present results on ScanRefer/Multi3DRefer and Nr3D/Sr3D. Vid-LLM achieves the best performance across all metrics on the two grounding benchmarks, surpassing all comparable 3D-based and video-based counterparts. These results demonstrate that the proposed Cross-Task Adapter, which effectively integrates semantic and geometric information, enables effective spatial reasoning and yields substantial gains on geometry-intensive tasks such as 3D visual grounding. For qualitative analysis, we visualize the 3D grounding results on the ScanRefer dataset in Fig. 4, which further demonstrates the 3D visual grounding capability of Vid-LLM. More qualitative visualizations for 3D VL tasks can be found in Appendix A.1.

4.3 COMPARISON WITH JOINT RECONSTRUCTION–REASONING MODELS

Overview. In addition to 3D vision–language reasoning, Vid-LLM also incorporates a reconstruction branch that provides geometric priors and metric-scale cues. This naturally raises the question of how different design choices for coupling reconstruction and reasoning affect performance when both tasks must be performed from a single video input. To provide a comprehensive analysis, we compare Vid-LLM with two representative categories of joint reconstruction–reasoning baselines: (i) simple concatenation pipelines that feed the 3D geometry reconstructed from video into a 3D multimodal LLM, and (ii) end-to-end architectures that integrate reconstruction and 3D VL reasoning within a single model.

Baseline. For the concatenation baselines, we construct pipelines that feed the predicted geometry information of VGGT into LLaVA-3D (Zhu et al., 2025) for 3D vision–language reasoning. Three variants of the concatenation pipeline are evaluated: (i) VGGT+LLaVA-3D, the direct combination of VGGT and LLaVA-3D; (ii) VGGT+LLaVA-3D[†], which introduces metric-scale alignment to the predictions of VGGT; (iii) VGGT+LLaVA-3D^{††}, which further fine-tunes LLaVA-3D using depth and camera poses predicted by VGGT as geometric supervision. For end-to-end joint-task baselines, we include Uni3DR² (Chu et al., 2024), an end-to-end framework that integrates a reconstruction



Figure 4: **Qualitative results of 3D visual grounding on the ScanRefer dataset.** The predicted 3D bounding boxes are visualized on point clouds reconstructed by our model.

Table 4: **Evaluation of 3D Visual Grounding on Nr3D and Sr3D.** Results are reported in grounding accuracy (%).

Method	Nr3D			Sr3D		
	Overall \uparrow	Hard \uparrow	View Dep \uparrow	Overall \uparrow	Hard \uparrow	View Dep \uparrow
ScanRefer	34.2	23.5	29.9	-	-	-
ReferIt3D	35.6	27.9	32.5	40.8	31.5	39.2
3DVG-Trans	40.8	34.8	34.8	51.4	44.9	44.6
MVT	55.1	49.1	54.3	64.5	58.8	58.4
ViL3DRel	62.6	55.6	59.8	72.5	68.1	58.0
Chat-3D v2	63.6	57.0	61.1	73.1	68.4	58.1
3D-VisTA	64.2	56.7	61.5	76.4	71.3	58.9
SceneVerse	64.9	57.8	56.9	77.5	71.6	62.8
Vid-LLM (Ours)	65.4	57.9	61.9	77.8	72.2	63.1

Table 5: **Comparison with end-to-end frameworks for joint 3D reconstruction and 3D VL reasoning.**

Method	Recon	3D VL Tasks			Time (s / scene) \downarrow
	ScanNet \uparrow	ScanQA \uparrow	Scan2Cap \uparrow	ScanRefer \uparrow	
<i>Concatenation models</i>					
VGGT+LLaVA-3D	-	24.6	35.1	31.6	2.7
VGGT+LLaVA-3D \dagger	0.591	42.1	50.9	47.3	2.7
VGGT+LLaVA-3D $\dagger\dagger$	0.591	41.6	48.2	45.9	2.7
<i>Joint-task models</i>					
Uni3DR 2	0.580	30.2	42.7	33.6	2.1
VGLLM-Rec	0.541	40.9	51.6	48.5	1.8
Vid-LLM (Ours)	0.582	45.7	53.2	59.8	1.6

\dagger denotes introducing real-scale;

$\dagger\dagger$ denotes training LLaVA-3D with 3D geometry predicted by VGGT

module with a 3D VL reasoning branch. Notably, Uni3DR 2 requires ground-truth camera poses as input, whereas Vid-LLM performs both tasks directly from video, making the comparison conservative in favor of Uni3DR 2 . We also include VGLLM-Rec, an extension of VGLLM (Zheng et al., 2025a). To support joint reconstruction and reasoning, we reconnect the original camera and depth prediction heads of VGGT to the geometry encoder in VGLLM, enabling VGLLM-Rec to generate geometric predictions in addition to performing 3D VL reasoning from video.

Result & Analysis. As shown in Tab. 5, VGGT+LLaVA-3D obtains very low 3D VL accuracy, indicating that relative-scale geometry cannot provide reliable cues for 3D VL reasoning. Building on this, VGGT+LLaVA-3D \dagger shows a clear performance gain once metric-scale alignment is applied. However, even with this setting, the concatenation baseline still underperforms Vid-LLM on all 3D VL tasks despite achieving a higher reconstruction score (0.591 vs. 0.582). This indicates that simply providing accurate reconstructed geometry to a 3D-LLM is insufficient and that effective geometry–semantics interaction is necessary for reliable reasoning performance. Furthermore, VGGT+LLaVA-3D $\dagger\dagger$ yields a slight drop in 3D VL accuracy compared with VGGT+LLaVA-3D \dagger , suggesting that training the 3D-LLM with noisy predicted geometry may introduce biases that degrade the semantic representations of the framework. In contrast to concatenation pipelines, end-to-end joint-task models avoid multi-stage processing and achieve lower inference latency, reducing runtime from 2.7 s/scene to 1.6–2.1 s/scene. From Tab. 5, we can observe that Vid-LLM achieves the best overall performance among the joint models on both reconstruction and 3D VL tasks. It marginally outperforms Uni3DR 2 in reconstruction quality on ScanNet (0.582 vs. 0.580) despite Uni3DR 2 having access to ground-truth camera poses. On the 3D VL tasks, Vid-LLM demonstrates a clear advantage, with an average relative improvement of 47.6% over Uni3DR 2 and 12.1% over VGLLM-Rec across ScanQA, Scan2Cap, and ScanRefer. Overall, Vid-LLM delivers the fastest inference speed and the best 3D VL performance, while also achieving the best reconstruction quality among joint-task models. These gains stem from our integrated architecture and the Cross-Task Adapter, which facilitates geometry–semantics interaction and allows the model to effectively leverage geometric cues during joint reasoning. More experimental results about reconstruction performance can be found in Appendix A.2.

Table 6: Ablation on Cross-Task Adapter (CTA) and Metric Depth (MD) Modules.

	3D VL Tasks			3D Recon
	ScanOA \uparrow	Scan2Cap \uparrow	ScanRefer \uparrow	scannet \uparrow
w/o CTA	33.7	36.6	34.1	0.402
CTA – Concat-SA	38.2	41.9	39.6	0.461
CTA – w/o Bridge (CA)	40.8	45.6	42.2	0.473
CTA – 4tokens	43.8	50.9	47.8	0.501
CTA – 8tokens	44.1	52.7	48.1	0.529
CTA – 16tokens (Ours)	45.7	53.2	48.4	0.582
CTA – 32tokens	45.2	52.8	47.6	0.564
w/o MD	29.6	35.7	33.9	-
MD – w/o Alignment	42.1	49.6	43.2	0.531
MD (Ours)	45.7	53.2	48.4	0.582

4.4 ABLATION STUDIES

Cross-Task Adapter. To assess the contribution of the Cross-Task Adapter, we compare several configurations: removing the CTA module (w/o CTA); in the setting without bridge tokens, applying self-attention to the concatenated T_{geom} and T_{lang} (CTA-Concat-SA) and performing cross-attention between the two feature sets (CTA-w/o Bridge (CA)); and finally using the full CTA with bridge tokens. We also analyze how different numbers of bridge tokens (4, 8, 16, and 32) affect model performance. As shown in Tab. 6, w/o CTA leads to the lowest performance on both tasks, confirming that a shared visual representation alone cannot jointly support reconstruction and 3D VL reasoning. Both CTA-Concat-SA and CTA-w/o Bridge(CA) show noticeable improvements, yet their effectiveness remains limited because neither design provides a stable shared latent space for passing geometric cues to semantic features. The configurations using the full CTA module (CTA-4/8/16/32tokens) all achieve clear performance improvements, since the bridge tokens provide a dedicated latent space that enables consistent geometry-semantic alignment and more effective cross-task interaction. Among different token counts, using 16 bridge tokens achieves the best balance between accuracy and model complexity.

Metric Depth Modules. Tab. 6 also reports ablations on the use of metric depth and our alignment strategy. Without metric depth supervision (w/o MD), scale ambiguity destroys geometric consistency and leads to near failure of 3D VL reasoning. Incorporating metric depth without alignment (MD – w/o Alignment) preserves metric scale but produces less accurate reconstruction, which in turn limits the performance of 3D VL tasks. By contrast, combining metric depth with our scale alignment strategy effectively exploits both global scale cues and relative structural details, yielding the most accurate reconstruction and consistently more reliable results on 3D VL tasks.

Two-Stage Training. Fig. 5 compares different training strategies to assess their impact on convergence and performance. Training all modules jointly without staging (Single-stage) converges slowly and stabilizes at a relatively high loss value, due to gradient interference across modules. Using a single teacher under the two-stage strategy (Two-Stage (One-Teacher)) offers limited supervisory signals, resulting in less effective optimization. Removing the relational loss during two-stage strategy (Two-Stage (w/o RelaLoss)) further slows convergence and reduces accuracy, highlighting the importance of enforcing cross-task consistency. In contrast, using the full two-stage strategy with dual-teacher supervision and relational consistency (Two-Stage (Ours)) achieves the fastest and achieves the lowest final loss.

5 CONCLUSION

In this work, we present Vid-LLM, a video-based 3D Multimodal Large Language Model (3D-MLLM). Our compact architecture extracts geometric cues from video and feeds them into the LLM through a 3D patch construction strategy to accomplish spatial reasoning. A central component of our framework is the Cross-Task Adapter that aligns 3D geometry priors with vision-language representations. This design enhances their integration into the MLLM and improves the robustness of reasoning under uncertain geometry. Together with a two-stage training strategy, our model achieves greater training stability and faster convergence. Extensive experiments on 3D vision-language

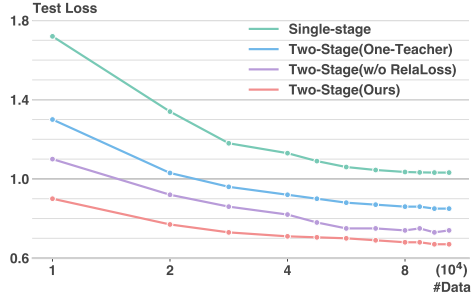


Figure 5: Test loss vs. data size across training strategies.

benchmarks demonstrate that Vid-LLM achieves state-of-the-art results on several benchmarks and remains competitive on the others, while ablation studies validate the effectiveness of each component.

6 REPRODUCIBILITY STATEMENT

We are committed to ensuring reproducibility. Part of our implementation is provided in the Supplementary Materials. Upon acceptance, we will release the complete code, datasets, and pretrained checkpoints to enable full verification of our results.

REFERENCES

- Panos Achlioptas, Ahmed Abdelreheem, Fei Xia, Mohamed Elhoseiny, and Leonidas Guibas. Referit3d: Neural listeners for fine-grained 3d object identification in real-world scenes. In *European conference on computer vision*, pp. 422–440. Springer, 2020a.
- Panos Achlioptas, Ahmed Abdelreheem, Fei Xia, Mohamed Elhoseiny, and Leonidas Guibas. Referit3d: Neural listeners for fine-grained 3d object identification in real-world scenes. In *European conference on computer vision*, pp. 422–440. Springer, 2020b.
- Daichi Azuma, Taiki Miyanishi, Shuhei Kurita, and Motoaki Kawanabe. Scanqa: 3d question answering for spatial scene understanding. In *proceedings of the IEEE/CVF conference on computer vision and pattern recognition*, pp. 19129–19139, 2022.
- Jonathan T Barron, Ben Mildenhall, Dor Verbin, Pratul P Srinivasan, and Peter Hedman. Mip-nerf 360: Unbounded anti-aliased neural radiance fields. In *Proceedings of the IEEE/CVF conference on computer vision and pattern recognition*, pp. 5470–5479, 2022.
- Shariq Farooq Bhat, Reiner Birkel, Diana Wofk, Peter Wonka, and Matthias Müller. Zoedepth: Zero-shot transfer by combining relative and metric depth. *arXiv preprint arXiv:2302.12288*, 2023.
- Wenxiao Cai, Iaroslav Ponomarenko, Jianhao Yuan, Xiaoqi Li, Wankou Yang, Hao Dong, and Bo Zhao. Spatialbot: Precise spatial understanding with vision language models. In *2025 IEEE International Conference on Robotics and Automation (ICRA)*, pp. 9490–9498. IEEE, 2025.
- Boyuan Chen, Zhuo Xu, Sean Kirmani, Brain Ichter, Dorsa Sadigh, Leonidas Guibas, and Fei Xia. Spatialvlm: Endowing vision-language models with spatial reasoning capabilities. In *Proceedings of the IEEE/CVF Conference on Computer Vision and Pattern Recognition*, pp. 14455–14465, 2024a.
- Dave Zhenyu Chen, Angel X Chang, and Matthias Nießner. Scanrefer: 3d object localization in rgb-d scans using natural language. In *European conference on computer vision*, pp. 202–221. Springer, 2020.
- Shizhe Chen, Pierre-Louis Guhur, Makarand Tapaswi, Cordelia Schmid, and Ivan Laptev. Language conditioned spatial relation reasoning for 3d object grounding. *Advances in neural information processing systems*, 35:20522–20535, 2022.
- Sijin Chen, Xin Chen, Chi Zhang, Mingsheng Li, Gang Yu, Hao Fei, Hongyuan Zhu, Jiayuan Fan, and Tao Chen. Ll3da: Visual interactive instruction tuning for omni-3d understanding reasoning and planning. In *Proceedings of the IEEE/CVF conference on computer vision and pattern recognition*, pp. 26428–26438, 2024b.
- Yilun Chen, Shuai Yang, Haifeng Huang, Tai Wang, Runsen Xu, Ruiyuan Lyu, Dahua Lin, and Jiangmiao Pang. Grounded 3d-llm with referent tokens. *arXiv preprint arXiv:2405.10370*, 2024c.
- Zhenyu Chen, Ali Gholami, Matthias Nießner, and Angel X Chang. Scan2cap: Context-aware dense captioning in rgb-d scans. In *Proceedings of the IEEE/CVF conference on computer vision and pattern recognition*, pp. 3193–3203, 2021.

- An-Chieh Cheng, Hongxu Yin, Yang Fu, Qiushan Guo, Ruihan Yang, Jan Kautz, Xiaolong Wang, and Sifei Liu. Spatialrgpt: Grounded spatial reasoning in vision-language models. *Advances in Neural Information Processing Systems*, 37:135062–135093, 2024a.
- An-Chieh Cheng, Hongxu Yin, Yang Fu, Qiushan Guo, Ruihan Yang, Jan Kautz, Xiaolong Wang, and Sifei Liu. Spatialrgpt: Grounded spatial reasoning in vision-language models. *Advances in Neural Information Processing Systems*, 37:135062–135093, 2024b.
- Tao Chu, Pan Zhang, Xiaoyi Dong, Yuhang Zang, Qiong Liu, and Jiaqi Wang. Unified scene representation and reconstruction for 3d large language models. *arXiv preprint arXiv:2404.13044*, 2024.
- Angela Dai, Angel X Chang, Manolis Savva, Maciej Halber, Thomas Funkhouser, and Matthias Nießner. Scannet: Richly-annotated 3d reconstructions of indoor scenes. In *Proceedings of the IEEE conference on computer vision and pattern recognition*, pp. 5828–5839, 2017.
- Rao Fu, Jingyu Liu, Xilun Chen, Yixin Nie, and Wenhan Xiong. Scene-llm: Extending language model for 3d visual understanding and reasoning. *arXiv preprint arXiv:2403.11401*, 2024.
- Yasutaka Furukawa, Carlos Hernández, et al. Multi-view stereo: A tutorial. *Foundations and trends® in Computer Graphics and Vision*, 9(1-2):1–148, 2015.
- Ziyu Guo, Renrui Zhang, Xiangyang Zhu, Yiwen Tang, Xianzheng Ma, Jiaming Han, Kexin Chen, Peng Gao, Xianzhi Li, Hongsheng Li, et al. Point-bind & point-llm: Aligning point cloud with multi-modality for 3d understanding, generation, and instruction following. *arXiv preprint arXiv:2309.00615*, 2023.
- Huy Ha and Shuran Song. Semantic abstraction: Open-world 3d scene understanding from 2d vision-language models. *arXiv preprint arXiv:2207.11514*, 2022.
- Yining Hong, Haoyu Zhen, Peihao Chen, Shuhong Zheng, Yilun Du, Zhenfang Chen, and Chuang Gan. 3d-llm: Injecting the 3d world into large language models. *Advances in Neural Information Processing Systems*, 36:20482–20494, 2023a.
- Yining Hong, Haoyu Zhen, Peihao Chen, Shuhong Zheng, Yilun Du, Zhenfang Chen, and Chuang Gan. 3d-llm: Injecting the 3d world into large language models. *Advances in Neural Information Processing Systems*, 36:20482–20494, 2023b.
- Haifeng Huang, Zehan Wang, Rongjie Huang, Luping Liu, Xize Cheng, Yang Zhao, Tao Jin, and Zhou Zhao. Chat-3d v2: Bridging 3d scene and large language models with object identifiers. *CoRR*, 2023a.
- Haifeng Huang, Yilun Chen, Zehan Wang, Rongjie Huang, Runsen Xu, Tai Wang, Luping Liu, Xize Cheng, Yang Zhao, Jiangmiao Pang, et al. Chat-scene: Bridging 3d scene and large language models with object identifiers. *Advances in Neural Information Processing Systems*, 37:113991–114017, 2024.
- Jiangyong Huang, Silong Yong, Xiaojian Ma, Xiongkun Linghu, Puhao Li, Yan Wang, Qing Li, Song-Chun Zhu, Baoxiong Jia, and Siyuan Huang. An embodied generalist agent in 3d world. *arXiv preprint arXiv:2311.12871*, 2023b.
- Shijia Huang, Yilun Chen, Jiaya Jia, and Liwei Wang. Multi-view transformer for 3d visual grounding. In *Proceedings of the IEEE/CVF Conference on Computer Vision and Pattern Recognition*, pp. 15524–15533, 2022.
- Xiaohu Huang, Jingjing Wu, Qunyi Xie, and Kai Han. Mllms need 3d-aware representation supervision for scene understanding. *arXiv preprint arXiv:2506.01946*, 2025.
- Baoxiong Jia, Yixin Chen, Huangyue Yu, Yan Wang, Xuesong Niu, Tengyu Liu, Qing Li, and Siyuan Huang. Sceneverse: Scaling 3d vision-language learning for grounded scene understanding. In *European Conference on Computer Vision*, pp. 289–310. Springer, 2024.

- Jihong Ju, Ching Wei Tseng, Oleksandr Bailo, Georgi Dikov, and Mohsen Ghafoorian. Dg-recon: Depth-guided neural 3d scene reconstruction. In *Proceedings of the IEEE/CVF International Conference on Computer Vision*, pp. 18184–18194, 2023.
- Bernhard Kerbl, Georgios Kopanas, Thomas Leimkühler, and George Drettakis. 3d gaussian splatting for real-time radiance field rendering. *ACM Trans. Graph.*, 42(4):139–1, 2023.
- Justin Kerr, Chung Min Kim, Ken Goldberg, Angjoo Kanazawa, and Matthew Tancik. Lrf: Language embedded radiance fields. In *Proceedings of the IEEE/CVF international conference on computer vision*, pp. 19729–19739, 2023.
- Johannes Kopf, Xuejian Rong, Jia-Bin Huang, Kevin Matzen, et al. Robust consistent video depth estimation. In *Proceedings of the IEEE/CVF Conference on Computer Vision and Pattern Recognition (CVPR)*, 2021.
- Seoyoung Lee and Joonseok Lee. Posediff: Pose-conditioned multimodal diffusion model for unbounded scene synthesis from sparse inputs. In *Proceedings of the IEEE/CVF Winter Conference on Applications of Computer Vision*, pp. 5007–5017, 2024.
- Yao-Chih Lee, Kuan-Wei Tseng, Guan-Sheng Chen, and Chu-Song Chen. Globally consistent video depth and pose estimation with efficient test-time training. *arXiv preprint arXiv:2208.02709*, 2022.
- Vincent Leroy, Yohann Cabon, and Jérôme Revaud. Grounding image matching in 3d with mast3r. In *European Conference on Computer Vision*, pp. 71–91. Springer, 2024.
- Bo Li et al. Llava-onevision: Easy visual task transfer. *arXiv preprint arXiv:2408.03326*, 2024.
- Ji Lin, Hongxu Yin, Wei Ping, Yao Lu, Pavlo Molchanov, Andrew Tao, Huizi Mao, Jan Kautz, Mohammad Shoeybi, and Song Han. Vila: On pre-training for visual language models. In *Proceedings of the IEEE/CVF Conference on Computer Vision and Pattern Recognition (CVPR)*, 2024.
- Philipp Lindenberger, Paul-Edouard Sarlin, Viktor Larsson, and Marc Pollefeys. Pixel-perfect structure-from-motion with featuremetric refinement. In *Proceedings of the IEEE/CVF International Conference on Computer Vision (ICCV)*, 2021.
- Liman Liu, Fenghao Zhang, Wanjuan Su, Yuhang Qi, and Wenbing Tao. Geometric prior-guided self-supervised learning for multi-view stereo. *Remote Sensing*, 15(8):2109, 2023. doi: 10.3390/rs15082109.
- Ze Liu, Han Hu, Yutong Lin, Zhuliang Yao, Zhenda Xie, Yixuan Wei, Jia Ning, Yue Cao, Zheng Zhang, Li Dong, Furu Wei, and Baining Guo. Swin transformer v2: Scaling up capacity and resolution. In *Proceedings of the IEEE/CVF Conference on Computer Vision and Pattern Recognition (CVPR)*, pp. 12009–12019, 2022.
- LLaVA Team. Llava-video: Video instruction tuning with synthetic data. *arXiv preprint arXiv:2410.02713*, 2024.
- Chenyang Ma, Kai Lu, Ta-Ying Cheng, Niki Trigoni, and Andrew Markham. Spatialpin: Enhancing spatial reasoning capabilities of vision-language models through prompting and interacting 3d priors. *Advances in neural information processing systems*, 37:68803–68832, 2024.
- Xiaojian Ma, Silong Yong, Zilong Zheng, Qing Li, Yitao Liang, Song-Chun Zhu, and Siyuan Huang. Sqa3d: Situated question answering in 3d scenes. *arXiv preprint arXiv:2210.07474*, 2022.
- Ben Mildenhall, Pratul P Srinivasan, Matthew Tancik, Jonathan T Barron, Ravi Ramamoorthi, and Ren Ng. Nerf: Representing scenes as neural radiance fields for view synthesis. *Communications of the ACM*, 65(1):99–106, 2021.
- Zak Murez, Tarrence van As, James Bartolozzi, Ayan Sinha, Vijay Badrinarayanan, and Andrew Rabinovich. Atlas: End-to-end 3d scene reconstruction from posed images. In *European Conference on Computer Vision (ECCV)*, 2020.

- Humza Naveed, Asad Ullah Khan, Shi Qiu, Muhammad Saqib, Saeed Anwar, Muhammad Usman, Naveed Akhtar, Nick Barnes, and Ajmal Mian. A comprehensive overview of large language models. *ACM Transactions on Intelligent Systems and Technology*, 16(5):1–72, 2025.
- Jia Ning, Chen Li, Zheng Zhang, Zigang Geng, Qi Dai, Kun He, and Han Hu. All in tokens: Unifying output space of visual tasks via soft token. In *Proceedings of the IEEE/CVF International Conference on Computer Vision (ICCV)*, 2023.
- Mingyang Ou, Heng Li, Haofeng Liu, Xiaoxuan Wang, Chenlang Yi, Luoying Hao, Yan Hu, and Jiang Liu. Mvd-net: Semantic segmentation of cataract surgery using multi-view learning. In *2022 44th Annual International Conference of the IEEE Engineering in Medicine & Biology Society (EMBC)*, pp. 5035–5038. IEEE, 2022.
- Vaishakh Patil, Christos Sakaridis, Alexander Liniger, and Luc Van Gool. P3depth: Monocular depth estimation with a piecewise planarity prior. In *Proceedings of the IEEE/CVF Conference on Computer Vision and Pattern Recognition (CVPR)*, 2022.
- Songyou Peng, Kyle Genova, Chiyu Jiang, Andrea Tagliasacchi, Marc Pollefeys, Thomas Funkhouser, et al. Openscene: 3d scene understanding with open vocabularies. In *Proceedings of the IEEE/CVF conference on computer vision and pattern recognition*, pp. 815–824, 2023.
- Alec Radford, Jeffrey Wu, Rewon Child, David Luan, Dario Amodei, Ilya Sutskever, et al. Language models are unsupervised multitask learners. *OpenAI blog*, 1(8):9, 2019.
- René Ranftl, Alexey Bochkovskiy, and Vladlen Koltun. Vision transformers for dense prediction. In *Proceedings of the IEEE/CVF International Conference on Computer Vision (ICCV)*, pp. 12159–12168, 2021.
- Jeremy Reizenstein, Roman Shapovalov, Philipp Henzler, Luca Sbordone, Patrick Labatut, and David Novotny. Common objects in 3d: Large-scale learning and evaluation of real-life 3d category reconstruction. In *Proceedings of the IEEE/CVF international conference on computer vision*, pp. 10901–10911, 2021.
- Ruilong Ren, Xinyu Zhao, Weichen Xu, Jian Cao, Xinxin Xu, and Xing Zhang. A survey of language-grounded multimodal 3d scene understanding. *Knowledge-Based Systems*, pp. 113650, 2025.
- Junha Roh, Karthik Desingh, Ali Farhadi, and Dieter Fox. Languagerefer: Spatial-language model for 3d visual grounding. In *Conference on Robot Learning*, pp. 1046–1056. PMLR, 2022.
- Paul-Edouard Sarlin, Daniel DeTone, Tomasz Malisiewicz, and Andrew Rabinovich. Superglue: Learning feature matching with graph neural networks. In *Proceedings of the IEEE/CVF Conference on Computer Vision and Pattern Recognition (CVPR)*, pp. 4938–4947, 2020.
- Johannes L Schonberger and Jan-Michael Frahm. Structure-from-motion revisited. In *Proceedings of the IEEE conference on computer vision and pattern recognition*, pp. 4104–4113, 2016.
- Jonas Schult, Francis Engelmann, Alexander Hermans, Or Litany, Siyu Tang, and Bastian Leibe. Mask3d: Mask transformer for 3d semantic instance segmentation. *arXiv preprint arXiv:2210.03105*, 2022.
- Nathan Silberman, Derek Hoiem, Pushmeet Kohli, and Rob Fergus. Indoor segmentation and support inference from rgb-d images. In *European conference on computer vision*, pp. 746–760. Springer, 2012.
- Jiaming Sun, Yiming Xie, Linghao Chen, Xiaowei Zhou, and Hujun Bao. Neuralrecon: Real-time coherent 3d reconstruction from monocular video. In *Proceedings of the IEEE/CVF conference on computer vision and pattern recognition*, pp. 15598–15607, 2021.
- Ashish Vaswani, Noam Shazeer, Niki Parmar, Jakob Uszkoreit, Llion Jones, Aidan N Gomez, Łukasz Kaiser, and Illia Polosukhin. Attention is all you need. *Advances in neural information processing systems*, 30, 2017.

- Jianyuan Wang, Minghao Chen, Nikita Karaev, Andrea Vedaldi, Christian Rupprecht, and David Novotny. Vggt: Visual geometry grounded transformer. In *Proceedings of the Computer Vision and Pattern Recognition Conference*, pp. 5294–5306, 2025a.
- Qianqian Wang, Yifei Zhang, Aleksander Holynski, Alexei A. Efros, and Angjoo Kanazawa. Continuous 3d perception model with persistent state. *arXiv preprint arXiv:2501.12387*, 2025b.
- Shuzhe Wang, Vincent Leroy, Yohann Cabon, Boris Chidlovskii, and Jerome Revaud. Dust3r: Geometric 3d vision made easy. In *Proceedings of the IEEE/CVF Conference on Computer Vision and Pattern Recognition*, pp. 20697–20709, 2024.
- Dong Wu, Zike Yan, and Hongbin Zha. Panorecon: Real-time panoptic 3d reconstruction from monocular video. In *Proceedings of the IEEE/CVF Conference on Computer Vision and Pattern Recognition*, pp. 21507–21518, 2024.
- Jiayang Wu, Wensheng Gan, Zefeng Chen, Shicheng Wan, and Philip S Yu. Multimodal large language models: A survey. In *2023 IEEE International Conference on Big Data (BigData)*, pp. 2247–2256. IEEE, 2023.
- Guangkai Xu, Wei Yin, Hao Chen, Chunhua Shen, Kai Cheng, and Feng Zhao. Frozenrecon: Pose-free 3d scene reconstruction with frozen depth models. In *2023 IEEE/CVF International Conference on Computer Vision (ICCV)*, pp. 9276–9286. IEEE, 2023.
- Jianing Yang, Alexander Sax, Kevin J Liang, Mikael Henaff, Hao Tang, Ang Cao, Joyce Chai, Franziska Meier, and Matt Feiszli. Fast3r: Towards 3d reconstruction of 1000+ images in one forward pass. In *Proceedings of the Computer Vision and Pattern Recognition Conference*, pp. 21924–21935, 2025.
- Lihe Yang, Bingyi Kang, Zilong Huang, Xiaogang Xu, Jiashi Feng, and Hengshuang Zhao. Depth anything: Unleashing the power of large-scale unlabeled data. In *Proceedings of the IEEE/CVF conference on computer vision and pattern recognition*, pp. 10371–10381, 2024.
- Shukang Yin, Chaoyou Fu, Sirui Zhao, Ke Li, Xing Sun, Tong Xu, and Enhong Chen. A survey on multimodal large language models. *National Science Review*, 11(12):nwae403, 2024.
- Duzhen Zhang, Yahan Yu, Jiahua Dong, Chenxing Li, Dan Su, Chenhui Chu, and Dong Yu. Mmllms: Recent advances in multimodal large language models. *arXiv preprint arXiv:2401.13601*, 2024a.
- Pan Zhang, Xiaoyi Dong, Yuhang Zang, Yuhang Cao, Rui Qian, Lin Chen, Qipeng Guo, Haodong Duan, Bin Wang, Linke Ouyang, et al. Internlm-xcomposer-2.5: A versatile large vision language model supporting long-contextual input and output. *arXiv preprint arXiv:2407.03320*, 2024b.
- Shangzhan Zhang, Jianyuan Wang, Yinghao Xu, Nan Xue, Christian Rupprecht, Xiaowei Zhou, Yujun Shen, and Gordon Wetzstein. Flare: Feed-forward geometry, appearance and camera estimation from uncalibrated sparse views. In *Proceedings of the IEEE/CVF Conference on Computer Vision and Pattern Recognition (CVPR)*, 2025.
- Yiming Zhang, ZeMing Gong, and Angel X Chang. Multi3drefer: Grounding text description to multiple 3d objects. In *Proceedings of the IEEE/CVF International Conference on Computer Vision*, pp. 15225–15236, 2023.
- Lichen Zhao, Daigang Cai, Lu Sheng, and Dong Xu. 3dvg-transformer: Relation modeling for visual grounding on point clouds. In *Proceedings of the IEEE/CVF International Conference on Computer Vision*, pp. 2928–2937, 2021.
- Wenliang Zhao, Yongming Rao, Zuyan Liu, Benlin Liu, Jie Zhou, and Jiwen Lu. Unleashing text-to-image diffusion models for visual perception. In *Proceedings of the IEEE/CVF International Conference on Computer Vision (ICCV)*, 2023.
- Duo Zheng, Shijia Huang, Yanyang Li, and Liwei Wang. Learning from videos for 3d world: Enhancing mllms with 3d vision geometry priors. *arXiv preprint arXiv:2505.24625*, 2025a.

- Duo Zheng, Shijia Huang, and Liwei Wang. Video-3d llm: Learning position-aware video representation for 3d scene understanding. In *Proceedings of the Computer Vision and Pattern Recognition Conference*, pp. 8995–9006, 2025b.
- Tinghui Zhou, Richard Tucker, John Flynn, Graham Fyffe, and Noah Snavely. Stereo magnification: Learning view synthesis using multiplane images. *arXiv preprint arXiv:1805.09817*, 2018.
- Chenming Zhu, Tai Wang, Wenwei Zhang, Jiangmiao Pang, and Xihui Liu. Llava-3d: A simple yet effective pathway to empowering llms with 3d capabilities. In *International Conference on Computer Vision (ICCV)(19/10/2025-23/10/2025, Honolulu, Hawai'i)*, 2025.
- Ziyu Zhu, Xiaojian Ma, Yixin Chen, Zhidong Deng, Siyuan Huang, and Qing Li. 3d-vista: Pre-trained transformer for 3d vision and text alignment. In *Proceedings of the IEEE/CVF International Conference on Computer Vision*, pp. 2911–2921, 2023.

A APPENDIX

In the Appendix, we provide the following experimental results:

- qualitative results and challenging cases of Vid-LLM in Appendix A.1;
- supplementary experiments on reconstruction performance in Appendix A.2;
- the use of large language models (LLMs) statement in Appendix A.3.

A.1 QUALITATIVE RESULTS AND CHALLENGING CASES

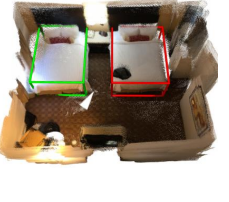
	Reconstruction	Question & Answer	Reconstruction	Question & Answer
3D Question Answering		<p>Q: How many chairs are there in the room ?</p> <p>A: Three.</p> <p>Q: Where is the monitor?</p> <p>A: In the corner of the desk against the wall.</p>		<p>Q: Where is the bed in the room ?</p> <p>A: On the right side of the room</p> <p>Q: What color are the curtains.</p> <p>A: Brown.</p>
3D Dense Captioning		<p>Q: Describe the room in detail.</p> <p>A: In the center of the meeting room, there is a light-colored conference table, surrounded by black conference chairs...</p>		<p>Q: Describe the Washbasin in detail.</p> <p>A: This is a brown washbasin, made entirely of light brown wood, with a circular washbasin in the center of the wash...</p>
3D Visual Grounding		<p>Q: There are two beds in the room. Give me the coordinates of these two beds.</p> <p>A:[1.13, 1.64, 0.35, 0.92, 0.03, 1.16], [1.13, 1.64, 0.35, 0.92, 0.03, 1.16]</p>		<p>Q: Give me the coordinates of the light brown wooden coffee table.</p> <p>A:[1.13, 1.64, 0.35, 0.92, 0.03, 1.16]</p>

Figure 6: **Qualitative Results.**

Qualitative Results. Fig. 6 presents reconstruction results on the ScanNet dataset, together with three representative 3D vision–language (3D VL) tasks. Specifically, it illustrates (1) 3D Question Answering, where the model answers queries on object counts, locations, and attributes from reconstructed scenes; (2) 3D Dense Captioning, which provides detailed semantic descriptions of rooms and key objects; and (3) 3D Visual Grounding, where the model localizes target objects in 3D space according to textual instructions. These qualitative results demonstrate the capability of Vid-LLM in scene reconstruction and 3D VL reasoning from video inputs.

Challenging Cases. Fig. 7 presents three challenging cases for Vid-LLM on 3D VL tasks. These scenes reflect typical failure modes of monocular video reconstruction, where limited camera viewpoints, reflective surfaces, or oblique viewing angles lead to incomplete geometry. As shown in examples (a) and (b), tasks that rely on explicit 3D structural information, such as instance counting or estimating 3D object extents for grounding, are directly affected by incomplete or unreliable geometry. In contrast, example (c) shows that Vid-LLM remains effective when sufficient 2D cues are present, due to the Cross-Task Adapter and bridge-token mechanism, which jointly align semantic and geometric information. These observations suggest that improving the reconstruction branch to enhance geometric fidelity could further strengthen the overall 3D VL performance, indicating a promising direction for future work.

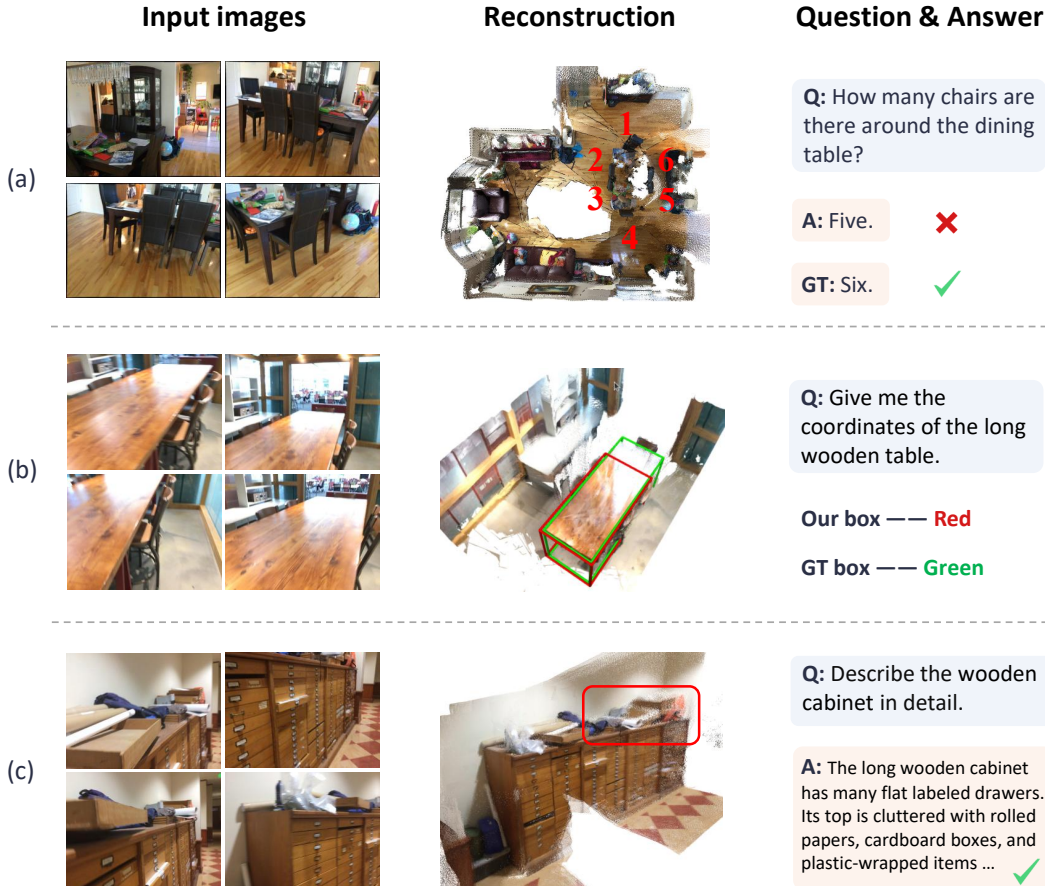


Figure 7: **Challenging Cases.** We present one challenging case for each 3D VL task—3D question answering (a), 3D visual grounding (b), and 3D dense captioning (c). (a) Due to limited camera viewpoints in the input video, one chair is only partially observed and consequently missing from the reconstruction, leading to an undercounted result. (b) The highly reflective tabletop results in unstable depth estimates and incomplete reconstruction, resulting in a predicted 3D box that is smaller than the ground truth. (c) The top surface of the cabinet is not well reconstructed because it appears only briefly and mostly from oblique angles, yet Vid-LLM nonetheless produces an accurate caption by leveraging rich 2D semantic cues.

Table 7: **Camera pose evaluation on Co3Dv2 and RealEstate10K.**

Method	Co3Dv2			RealEstate10K
	RRA@15↑	RTA@15↑	mAA(30)↑	mAA(30)↑
COLMAP+SG (Sarlin et al., 2020)	36.1	27.3	25.3	45.2
PixSfM (Lindberger et al., 2021)	33.7	32.9	30.1	49.4
PoseDiff (Lee & Lee, 2024)	80.5	79.8	66.5	48.0
DUST3R (Wang et al., 2024)	94.3	88.4	77.2	61.2
MASt3R (Leroy et al., 2024)	94.6	91.9	81.8	76.4
FLARE (Zhang et al., 2025)	95.4	83.6	78.4	75.3
Fast3R (Yang et al., 2025)	96.2	81.6	75.0	72.7
CUT3R (Wang et al., 2025b)	95.7	84.5	73.3	77.1
VGGT (Wang et al., 2025a)	97.3	93.3	89.6	83.8
Vid-LLM (Ours)	<u>96.8</u>	93.4	<u>88.5</u>	<u>83.1</u>

Table 8: **Depth estimation results on the NYU Depth v2 dataset.** [†] Model outputs are in relative scale; we align them to the ground-truth metric scale prior to evaluation.

Method	$\delta 1 \uparrow$	AbsRel \downarrow	RMSE \downarrow	log10 \downarrow
DPT (Ranftl et al., 2021)	0.904	0.110	0.357	0.045
P3Depth (Patil et al., 2022)	0.898	0.104	0.356	0.043
SwinV2-L (Liu et al., 2022)	0.949	0.083	0.287	0.035
AiT (Ning et al., 2023)	0.954	0.076	0.275	0.033
VPD (Zhao et al., 2023)	0.964	0.069	0.254	0.030
ZoeDepth (Bhat et al., 2023)	0.953	0.075	0.270	0.032
DepthAnything (Yang et al., 2024)	0.984	0.056	0.206	0.024
VGGT [†] (Wang et al., 2025a)	0.989	0.022	0.103	0.011
Vid-LLM(Ours)	0.987	0.025	0.109	0.010

Table 9: **Reconstruction results on the ScanNet dataset.** [†] Model outputs are in relative scale; we align them to the ground-truth metric scale prior to evaluation.

Method	GT cams	Comp \downarrow	Acc \downarrow	Recall \uparrow	Prec \uparrow	F-score \uparrow
MVDNet (Ou et al., 2022)	✓	0.040	0.240	0.831	0.208	0.329
GPMVS (Liu et al., 2023)	✓	0.031	0.879	0.871	0.188	0.304
Atlas (Murez et al., 2020)	✓	0.062	0.128	0.732	0.382	0.499
NeuralRecon (Sun et al., 2021)	✓	0.106	0.073	0.428	0.592	0.494
DG-Recon (Ju et al., 2023)	✓	0.085	0.039	0.476	0.675	0.521
PanoRecon (Wu et al., 2024)	✓	0.089	0.064	0.530	0.656	0.584
RCVD (Kopf et al., 2021)	×	0.161	0.425	0.164	0.109	0.125
GCVD (Lee et al., 2022)	×	0.175	0.278	0.178	0.146	0.147
Colmap (Schonberger & Frahm, 2016)	×	0.142	0.367	0.119	0.267	0.178
FrozenRecon (Xu et al., 2023)	×	0.092	0.085	0.436	0.336	0.410
DUST3R (Wang et al., 2024)	×	0.243	0.179	0.284	0.657	0.387
VGGT [†] (Wang et al., 2025a)	×	0.067	0.044	0.658	0.891	0.580
Vid-LLM(Ours)	×	0.071	0.042	0.634	0.885	0.582

A.2 SUPPLEMENTARY EXPERIMENTS ON RECONSTRUCTION

Overview. Since the reconstruction branch not only provides 3D cues for the 3D-MLLM but also explicitly produces point clouds that can serve downstream applications, it is important to assess its individual performance. To evaluate the 3D modeling capability of Vid-LLM, we assess three tasks: camera pose estimation, depth prediction, and point-cloud reconstruction. Depth prediction is crucial to real-scale reconstruction, and together with poses it determines the quality of the recovered point clouds. Following standard protocols, we evaluate poses on Co3Dv2 (Reizenstein et al., 2021) and RealEstate10K (Zhou et al., 2018), depth on the indoor NYU Depth v2 dataset (Silberman et al., 2012), and point-cloud reconstruction on ScanNet (Dai et al., 2017), ensuring consistency with the 3D vision-language benchmarks introduced earlier. Depth and reconstruction evaluations require the model to predict real-scale geometric outputs, while camera pose estimation is scale-invariant.

Baseline. For 3D reconstruction, we evaluate three subtasks: (i) camera pose estimation, where we compare against geometry-based optimization methods including COLMAP+SG and PixSfM, as well as state-of-the-art learning-based approaches such as PoseDiff, DUST3R, MAST3R, FLARE, Fast3R, and CUT3R; (ii) monocular depth estimation, where we benchmark against DPT, P3Depth, SwinV2-L, AiT, VPD, ZoeDepth, and DepthAnything; and (iii) point-cloud reconstruction, where we consider pose-dependent methods such as MVDNet, GPMVS, Atlas, NeuralRecon, DG-Recon, and PanoRecon, together with pose-free approaches including RCVD, GCVD, COLMAP, FrozenRecon, and DUST3R, ranging from traditional multi-view geometry to modern learning-based techniques. We further benchmark against VGGT, which serves as both a high-performing reconstruction model and as the reconstruction teacher in our framework.

Result & Analysis. Across the three benchmarks, Vid-LLM achieves reconstruction quality comparable to VGGT while operating in an end-to-end real-scale setting. On camera pose estimation (Tab. 7), Vid-LLM attains results close to VGGT on both Co3Dv2 and RealEstate10K and slightly

outperforms it on RTA@15 for Co3Dv2. On NYU Depth v2 and ScanNet (Tab. 8 and Tab. 9), VGGT requires an explicit scale-alignment step to match the metric ground truth, whereas Vid-LLM predicts real-scale depth and point clouds in an end-to-end manner. In this setting, Vid-LLM achieves lower log10 error on NYU and higher F-score and accuracy on ScanNet than VGGT, indicating that its real-scale geometry remains competitive against the teacher model. Vid-LLM also surpasses all other models that predict real-scale outputs. Overall, these results confirm that its reconstruction module delivers consistent and reliable geometric performance.

A.3 THE USE OF LARGE LANGUAGE MODELS (LLMs) STATEMENT

Parts of the language in this manuscript were polished with the assistance of Large Language Models (LLMs). The authors have carefully reviewed and verified all LLM-assisted text to ensure accuracy and appropriateness. The intellectual contributions, ideas, and conclusions presented in this work are entirely those of the authors.